International Shipbuilding Progress 60 (2013) 345–374
DOI 10.3233/ISP-130097
IOS Press

Hydrodynamic mechanisms controlling cavitation erosion

Göran Bark * and Rickard E. Bensow
Chalmers University of Technology, Gothenburg, Sweden

In this paper we consider development of cavitation erosion having its origin in sheet cavitation. The discussion includes generation of cloud cavitation from sheet cavitation and how a cloud collapse can be enhanced by energy cascading from the collapse of a glassy sheet cavity into the collapse of a cloud. A decomposition of the cavitation process into crucial parts results in formulation of a conceptual model for description and analysis of the generation of erosion by mixed glassy and cloud cavitation.

Keywords: Sheet and cloud cavitation, cavitation erosion

1. Background and present approach

We start by a brief review of the generic example of erosive cavitation shown in Fig. 1. This cavitation in the root region of a propeller develops from a large sheet cavity generating typically three erosion regions, of which two are shown in the figure. The root cavity is beneficial for isolation of generally relevant events and is assumed not to limit the analysis and conclusions.

The propeller is operating in a homogeneous flow with an inclined shaft (8 degree inclination angle). Thus, the propeller blades experience an unsteady flow due to the shaft inclination only. The cavity in frame 1 is a narrow sheet cavity that was initially attached to a line close to the leading edge but has now started to move slowly downstream, frame 2. The closure region is moving upstream as a jet flow is filling the sheet. This jet that can contribute significantly to the filling, started as an undisturbed re-entrant jet, but is later enhanced by flows induced by the shed vortices and by the increasing collapse forcing pressure on the blade. The jet is now almost as thick as the sheet cavity. Momentum and shear interaction between the filling flow and the flow outside the sheet cavity generate shedding of vortex cloud cavitation in the closure region.

Of the two erosive collapses shown in the frames. the first appearing one is the collapse of the glassy part, almost captured by frame 3, and the second is the collapse of the cloud around frame 7. The collapse of the glassy sheet cavity contributes to

*Corresponding author. E-mail: bark@chalmers.se.

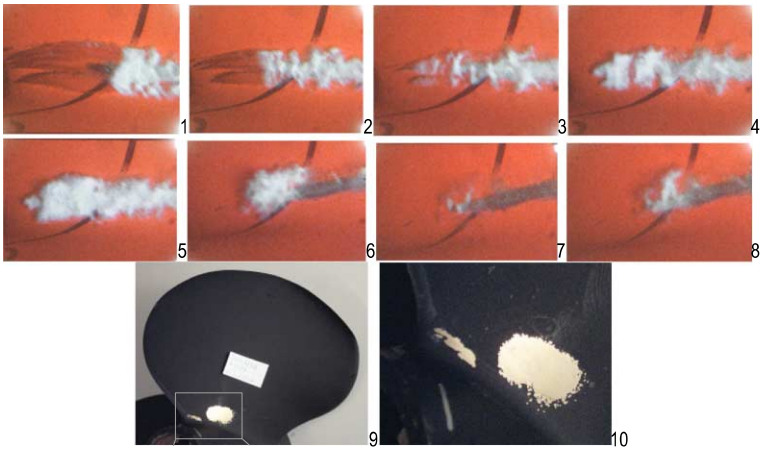

Fig. 1. Frames 1–8 are samples from a high-speed film of a sheet cavity in the root region of a propeller in the SSPA cavitation tunnel. The smaller white patch in photos 9 and 10 shows the wear of soft paint due to collapses of the glassy sheet cavity with the attached bubble cloud, frame 3, and the larger patch is created by the collapses of the clouds in frames 5 and 8. Frame 8 shows the rebound of the cloud in frame 5. From [1]. (Colors are visible in the online version of the article; http://dx.doi.org/10.3233/ISP-130097.)

the erosion (paint wear) in the upstream patch in photos 9 and 10 and the cloud collapse generates the larger downstream patch. The large extent of this patch is due to scattering in time and space of the cloud collapses, and the fact that also the rebounded cloud shown in frame 8 collapses in the downstream region of this patch.

Assessments of propeller erosion are often based on model scale experiments analysed according to:

(a) visual assessment of the wear/erosion of a soft paint being exposed during a certain time to the cavitation, as shown in Fig. 1, and by
(b) visual assessment of the cavitation aggressiveness based on high-speed video recording of cavity collapses.

None of the above methods are strictly quantitative, although a quantitative assessment of the cavitation aggressiveness is usually made in both methods. The mechanical properties of the soft paint is a rough scaling to the full-scale propeller material. Without supplementary observations of the cavitation the bare paint method does not reveal much information about the hydrodynamics behind the erosion. Assessment of propeller erosion by paint tests, empirically calibrated by model to full scale correlation of erosion data, is nevertheless shown to be reliable in many cases.

High-speed video analysis of the cavitation, brings useful information about the hydrodynamics, but in this method the erosion sensor is replaced by an approximate analysis of the collapse kinematics. The video and paint methods do, however, sup-

plement each other, partly because they usually fail for different reasons. There is a third method, based on recording of the structure borne noise created by cavity collapses on a propeller blade. This has been applied at full-scale propellers by Boorsma and Fitzsimmons [7]. A new technique is also advanced numerical simulation of the cavitation process, including sometimes collapse pulses [5,9,17,19,20].

Principles for erosion assessment based on cavitation kinematics and statistics are described in the EROCAV observation handbook [1], supplemented by Grekula and Bark [11], Grekula [10] and Bark et al. [3]. These guidelines were primarily written for analysis of experimental model or full scale data, but with also numerical simulations in mind.

In the present paper we extend the decomposition of the cavitation process that was introduced by Bark et al. [3], in order to show the processes that have to be captured for experimental and numerical erosion predictions. We notice particularly that partly glassy sheet cavities occur at both model and full-scale propellers, Figs 1 and 2. Because, however, a sheet cavity at full scale develops in a more turbulent flow the sheet may start, partly at least, as a sheet of travelling bubbles and accordingly there can be a tendency that sheet cavities at full scale contain more cloud formations compared to model scale. The behavior of mainly glassy sheet cavities, and particularly their partial transformation to cloud cavitation, will be shown to be important for erosion.

The study is primarily based on experimental recordings at model scale, but numerical simulations are applied for supplementary visualization of some events that are difficult to evaluate from experimental recordings. Implicit Large Eddy Simulations (ILES) is assumed to capture such events [6].

By analysis of high-speed video data of cavitation on a propeller and foils certain processes, such as collapse energy cascading and focusing, have been identified as "main processes" in the development of erosive collapses. Partly idealized definitions of the main processes, and related sub processes, are summarized into ten "Analysis Models", to support analysis and description of collapses of cavities, such as the one in Fig. 1.

Imbedded in the Analysis Models are hypotheses relating to the involved physics. The main processes and their sub processes constitute a particular decomposition of the total cavitation process into observable processes that have to be captured in experiments and in numerical simulations. The main and sub processes also form a nomenclature for description of erosive cavitation, and for relating erosion to large scale hydrodynamics and design selections.

The Analysis Models include large to moderately small scales, excluding thus the very final, fast and most small-scale process involved in transfer of collapse energy to the solid body. This very late process can partly be related to the stopping and reversing of the collapse motion into a rebound of the cavity. Although important, the details of the smallest scales are excluded from the analysis, because they cannot be resolved by numerical or experimental methods that are applicable to propeller conditions. The Analysis Models are presented in five sections:

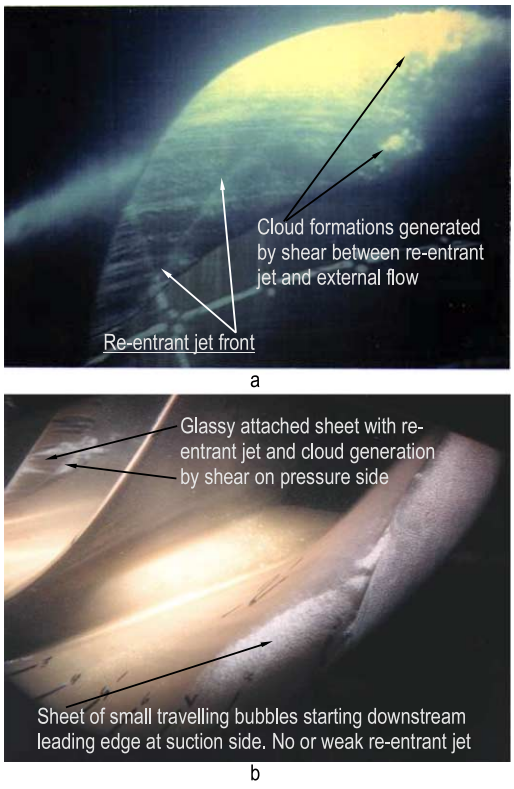

Fig. 2. Cavitation on full scale propellers. (a) Mainly glassy sheet cavity with re-entrant jet (on the suction side). Photo by SSPA. (b) Glassy sheet cavity with re-entrant jet on the pressure side (*left*) and sheets of travelling bubbles, i.e. a type of cloud cavitation, on the suction side (*right*). The bubbly sheet far to the right starts close to the leading edge. In both glassy sheet cavities with re-entrant jets the cloud cavitation is mainly created by shear between re-entrant jet and external flow. Photo by DTMB. From ITTC [15] and [16]. (Colors are visible in the online version of the article; http://dx.doi.org/10.3233/ISP-130097.)

- Erosion by sheet cavitation.
- Focusing of collapse energy.
- Primary and secondary cavities.
- Asymmetry and vortex formation.
- Generalized collapse and rebound.

2. Erosion by sheet cavitation

Although the stress resulting in erosion in the solid body is related to a very late part of the collapse, the accumulation of the collapse energy involved in the final impact can start during the early collapse motion. However, accumulated kinetic

energy can also be lost during the collapse by disintegration of the cavity or by temporal retardation of the collapse.

Based on the simplified ideas summarized above and to create a link to the global flow and design parameters the EROCAV analysis was focused on the large-scale and early development of the collapse motion. Data to be analyzed in this approach are collapse pulse data and the collapse kinematics.

The type of cavitation associated with erosion is particularly cloud cavitation. This cloud is however in many cases created by sheet cavitation, which may be mainly glassy or partly filled with cloud cavitation. Hydrodynamically generated cavities usually contain some cloud formations during part of their existence. If the cavity at the start of its collapse contains a very small amount of cloud formations it may be referred to as an almost glassy cavity if the cloud is small compared to the glassy part. Two examples of almost glassy cavities are found in Figs 2 and 7.

We argue below for a hypothesis stating that a sheet cavity collapse can contribution to erosion by cascading collapse energy to a cloud, the enhanced collapse of which is finally assumed to create the erosion. This cloud cavitation is usually generated by one or more of the following processes:

(a) By direct excitation of cavitation nuclei, e.g. in the growth of a bubble sheet in a turbulent boundary layer, Figs 2(b) and 3, or by the pressure close to a vibrating body.
(b) By the shear and mixing flow created when a cavity is filled by re-entrant jet flow, or by a reversed flow of other origin, Figs 5 and 12, [8].
(c) By a fast rebound of a glassy cavity, due to instability and the rarefaction phase of the collapse pulse. Figure 7, frame 7064.

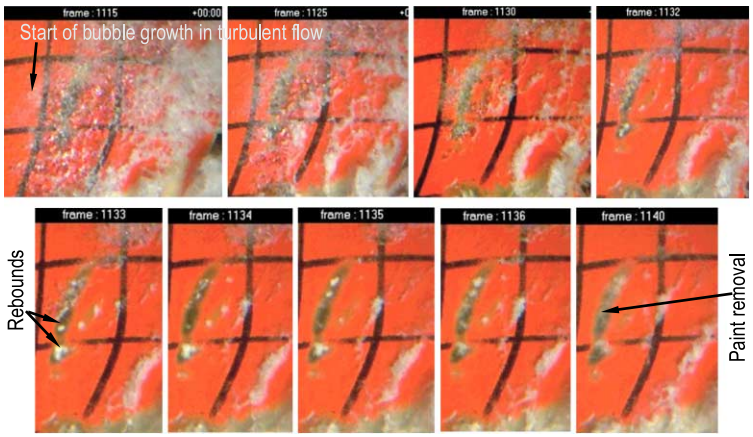

Fig. 3. Sheet of travelling bubbles performing erosive collapses on a propeller blade. Flow from left to right. Notice dispersion into several collapse points, indicated by the intensely white rebound spots in frames 1133–1135. SSPA cavitation tunnel. From Bark et al. [3]. (Colors are visible in the online version of the article; http://dx.doi.org/10.3233/ISP-130097.)

When a cloud sheet is created according to point (a) the sheet will more or less become a sheet of travelling bubbles, Figs 2(b) and 3. This implies that re-entrant jets will be subdued, as in the case of Fig. 3, or not at all develop. The bubbles in these cloud sheets are usually much larger compared to those created by shear, and particularly by a fast rebound. The smallest bubbles created by a fast rebound form a dense opaque bubble suspension, more white than other cloud cavities, because of high diffuse reflectivity [21].

Based on Bark et al. [2] we condense into Analysis models 1 and 2 observations and hypotheses about the generation of erosion by coupled collapses of glassy sheets and cloud cavitation and some processes to notice.

Analysis model 1 (Cascading of collapse energy from a glassy sheet cavity to cloud cavities).

1. The collapse of a glassy cavity can contribute to erosion by cascading part of its collapse energy into the collapse motion of an attached or nearby small bubble cloud, which then performs the final focusing and transfer of the energy to the solid body.
2. Typically the collapse motion of a glassy cavity will, as shown in Fig. 4(b), bring the attached cloud to finally fill the entire vapor region, containing also some gas. After this filling, frames 6–9 in Fig. 4(b), the collapse front continues inwards in the cloud, cascading the increasing energy density to the collapse motion of some last collapsing bubbles, some of which being close to or possibly in contact with the body surface. The collapse motion is assumed to be stopped by compression of the cavity content and/or the surroundings. The stopping may be controlled by an impact on the body surface as well. The compression is assumed to finally force the "compression rebound" of the cavity that follows.
3. Observations indicate also existence of possibly relevant energy cascading, by acoustic interaction, to small clouds near the sheet collapse.
4. In cases 2 and 3 the final focusing and erosion is assumed to be generated by the small bubble clouds. The smallest clouds forced to erosive collapses by a sheet cavity collapse are assumed to not necessarily be erosive without the energy gained from the collapse of the sheet cavity.

Analysis model 2 (Characteristic processes controlling erosion by cloud cavitation).

1. *Inhomogeneity of bubble distribution in the cloud*, caused by inhomogeneous nuclei distribution and the cloud generation and mixing processes. This results in more than one collapse point, scattered over cavitation cycles. The collapse energy is dispersed in space and time, and erosion is reduced, Fig. 3 (frame 1132) and Fig. 5 (frames 1132 and 5967).

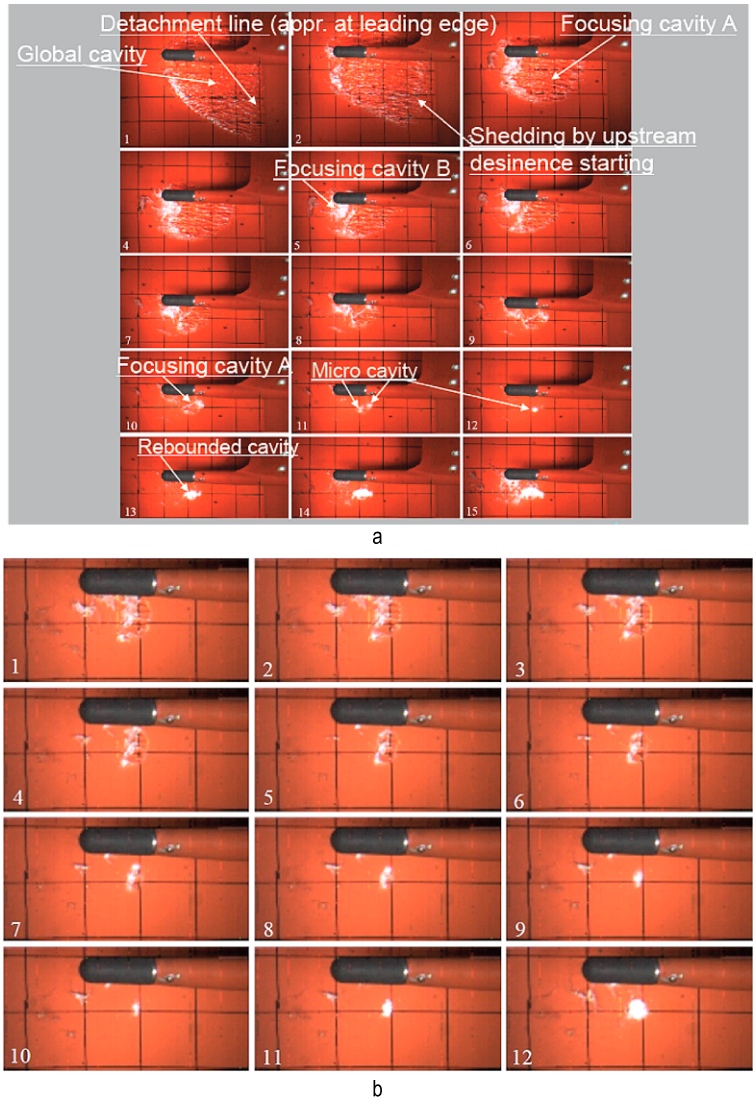

Fig. 4. Collapse of an almost glassy travelling sheet cavity on a twisted stationary foil in unsteady flow generated by an oscillating foil upstream of the shown foil. Flow from right to left, 5 m/s. Samples from high-speed film. (a) Illustration of the concepts of "global", "main focusing" and "micro focusing" cavities introduced in Analysis model 3. (b) Increased time and spatial resolution of the final part of the collapse and early rebound of the focusing cavity A. Time interval between frames 8, 9, 10 and 11 is 1/30,000 s. SSPA cavitation tunnel. From Bark et al. [1]. (Colors are visible in the online version of the article; http://dx.doi.org/10.3233/ISP-130097.)

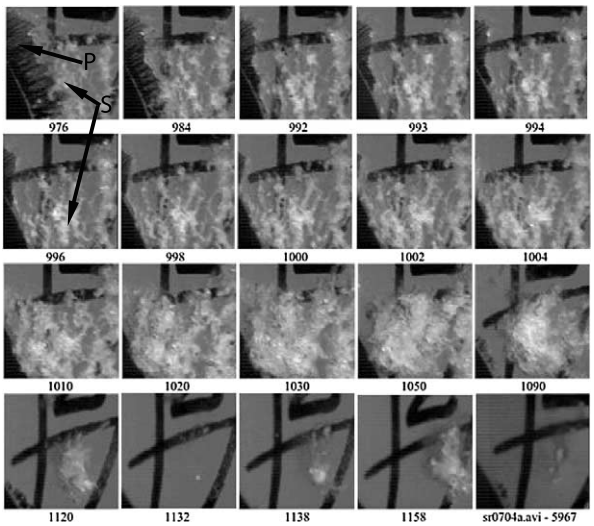

Fig. 5. Propeller operating in inclined flow. Flow from left to right. Frames from high-speed video recording. Unit step interval of frame number equals $1/90{,}000$ s. Upstream moving collapse of primary sheet cavity (P) and growth and merging of secondary cloud cavitation (S) into vortex group cavitation as described by Foeth [8]. The rebound of the vortex group cavitation is shown in frames 1138 and 1158. The last frame is taken from a different recording at the same test. The different collapse positions in frames 1132 and 5967 show a typical collapse position scatter. SSPA cavitation tunnel. From Bark et al. [2].

2. *Synchronization of different parts of cloud cavities*, by flow and pressure fields. This synchronization controls the extent to which different parts of a total cloud contribute to erosive collapses. The tiny clouds attached to the glassy cavity in Fig. 4(b) are effectively synchronized by the converging flow of the glassy cavity collapse.
3. *Lifting of a cloud cavitation from the body surface* can reduce erosion. This can occur if the cloud develops in a vortex shedding, as in Figs 5, 12(a) and 13(e) and (g). It can also happen at the closure of a sheet cavity making an upstream moving collapse, Fig. 12(g).
4. Development of a shed vortex cavity into a horseshoe vortex cavity can enhance the erosion by increased synchronization and focusing of the cloud collapse.

3. Focusing of collapse energy

The flow converging towards a point in a spherically symmetric collapse of a cavity results in a kinematic focusing into a local and temporal maximum of kinetic energy on the cavity interface a short time before the collapse is finished. Part of the kinetic energy released in the collapse motion is transferred to potential energy in the

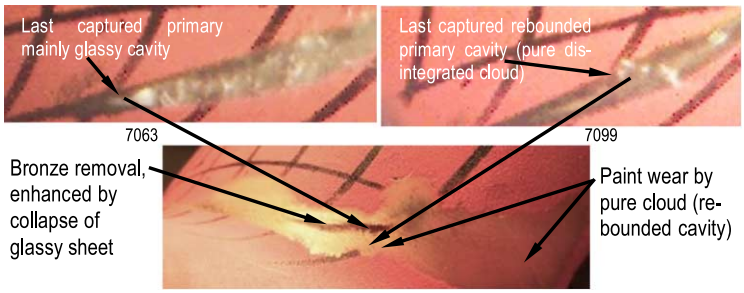

Fig. 6. Erosion by the cavitation in Fig. 7. (Colors are visible in the online version of the article; http://dx.doi.org/10.3233/ISP-130097.)

compressed cavity content and surroundings. It is noted that even a non-accelerating and non-converging collapse motion of e.g. a planar liquid interface, with possibly imbedded bubbles, hitting a solid body means a focusing of collapse energy at the impact.

Energy focusing, being addressed by other authors as well, was formulated in the EROCAV handbook for analysis of complex collapse processes, including sequences of collapses. Present discussion is mainly limited to the basic single collapses and the concept of energy focusing is then described in Analysis model 3.

Analysis model 3 (Focusing and cascading of collapse energy – focusing cavities and collapses).

1. *A global cavity* is a cavity of any type and configuration from which the main focusing cavity defined in the next point is formed. An example is the root cavity in Fig. 7 that develops from a global sheet cavity, initially covering a large part of the propeller blade and later disintegrates into three erosive focusing cavities, one of which is the root cavity.
2. *A main focusing cavity* is a part of the global cavity that performs a main focusing collapse motion (ideally towards a point), to the size below which it cannot anymore be described by the resolution applied, e.g. the sheet in frame 7046 of Fig. 7 and cavity A in frames 3–5 of Fig. 4(a). More than one focusing cavities can coexist, A and B in Fig. 4(a).
3. *A micro focusing cavity* is a cavity continuing the energy focusing started by the main focusing cavity, into time and spatial scales that are not resolved in detail by the applied technique.
   The micro focusing cavity may be a regenerating cloud continuing the energy focusing into the final collapse, Fig. 4(b), frames 9–10. (This collapse is followed by a fast rebound to a dense cloud of very small bubbles, Fig. 4(b), frames 11–12. See also Analysis model 10.)
4. The focusing may proceed by momentum forced energy cascading from the collapse of a glassy sheet cavity to an attached cloud (Fig. 4(b), frames 1–9),

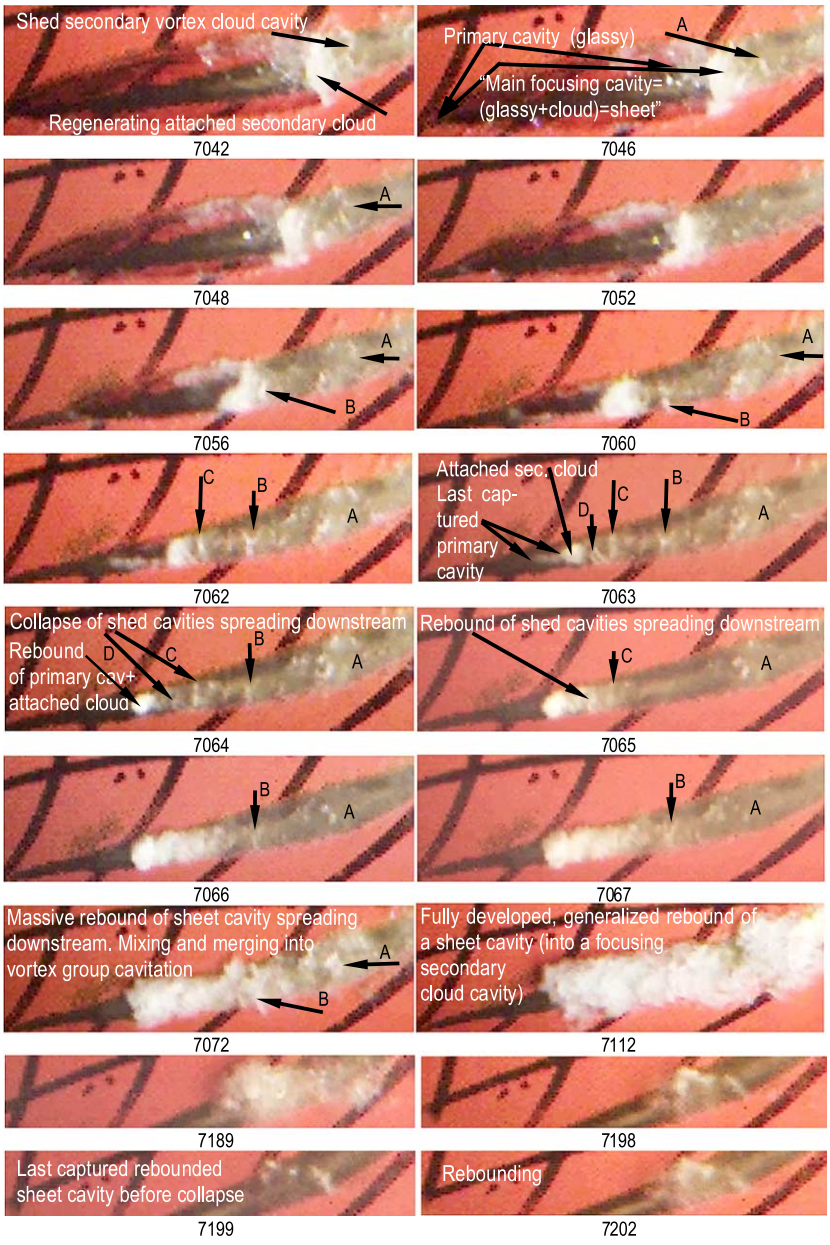

Fig. 7. Collapse of a root sheet cavity and its generalized rebound on the propeller in inclined flow. Flow from left to right, 9 m/s. Frames from high-speed video. Unit step in frame number equals 1/75,000 s. Erosion in Fig. 6. (See also discussion prior to Analysis model 9.) SSPA cavitation tunnel. (Colors are visible in the online version of the article; http://dx.doi.org/10.3233/ISP-130097.)

or by acoustic interaction to nearby clouds, e.g. to the shed clouds downstream the collapse point in Fig. 7, frames 7064–7066. In the limit of a homogeneous cloud the focusing may proceed continuously into the micro state, but often the cloud will split into more than one collapse point, Fig. 3.

5. Depending on the selected resolution there may be cascading processes in the micro focusing state that are not captured. Although the assessment quality usually increases with recording resolution, it is assumed that approximate and relative assessments of erosion risks sometimes can be made also from recordings that do not resolve the latest part of the collapse.

For typical propeller erosion the main focusing cavities are usually large enough to be easily detected at a model test. In other applications, with very long operating time, high surrounding pressure or soft materials, erosion can be generated also by very small cavities.

The initiation of a focusing cavity starts by transformation of at least a part of the global cavity into a transient state developing into a focusing motion. Typical, partly interrelated processes, for formation of focusing cavities are described in Analysis model 4.

Analysis model 4 (Formation of focusing cavities). Focusing cavities are usually formed by:

1. *Direct creation of a travelling cavity*, i.e. of a cavity, the upstream edge of which is not fixed to a stationary starting/detachment line. A basic example is a single travelling cavitation bubble, Fig. 9, and the sheet of travelling bubbles in Fig. 2(b).
2. *Shedding* of a part of an attached or travelling cavity, or a general disintegration due to e.g. an irregular thickness. The shedding can also develop due to local filling of a sheet cavity by re-entrant jets, cavity B in Figs 4(a) and 12(a)–(d).
3. *Upstream or local desinence*, i.e. the onset of cavitation desinence at the upstream starting line of an initially attached cavity, or elsewhere. An example is the sheet cavity in frame 2 of Fig. 4(a) shed from the leading edge due to a decreasing angle of attack.
4. The *upstream moving collapse* of an attached cavity. A basic example is the sheet cavity attached to an upstream position during its entire existence and is collapsing by upstream motion of its closure line, as the sheet cavity P in Fig. 5 and the sheet cavity in Fig. 12.
5. *Generation of secondary cavities*, usually of cloud type. The typical generation processes are shear, followed by shedding and merging, and by rebounds, as discussed in next section.

4. Primary and secondary cavities

The tiny, merging and synchronizing, cloud formations assumed to be critical in the erosive case in Fig. 4(b) are examples of secondary cavitation. Secondary cavita-

tion, being usually of cloud type, is observed to play a major role in erosion, Bark et al. [2].

Analysis model 5 (Primary cavities). A *primary cavity* is the glassy, cloud or mixed cloud and glassy cavity that remains when secondary cavitation volumes, according to Analysis model 6 below, has been subtracted from the total cavity volume.

Examples of primary cavities are the sheet of travelling bubbles in Fig. 2(b), most of the bubble sheet in Fig. 3, the glassy part of the mixed sheet cavity in frames 7042 and 7046 in Fig. 7 and the glassy part P of the sheet cavity in Fig. 5.

Analysis model 6 (Secondary cavities). A *secondary cavity* is created by the flow and pressure induced by certain interface motions of the primary cavity, particularly collapse motions, re-entrant jets or similar flows. Secondary cavitation processes resulting from collapse motion can alternatively be interpreted as rebounds of the cavity, an ordinary "compression rebound" or a "vortex rebound". These two rebound types are parts of a *generalized rebound* as will be described in the Analysis models 7 and 10. Secondary cavities are primarily generated by:

1. *Shear and momentum interaction* between a re-entrant jet and the external flow. This interaction generates a secondary vortex cavity, usually of cloud type, here defined also as a *vortex rebound of a sheet cavity*, or a part of it. The clouds usually created are:
   (a) A cloud of very small extent, attached to the shear region of the sheet cavity, in which the cloud regenerates and finally in the collapse gains collapse energy from the sheet cavity, frames 1–8 in Fig. 4(b) and frame 247 in Fig. 9.
   (b) A cloud of moderate extent, attached to the shear region of the sheet cavity, in which the cloud regenerates and gains collapse energy from the sheet cavity collapse, as in the downstream part of the sheet in frame 7042 of Fig. 7 and frames 1–2 of Fig. 1. Some shedding usually occurs.
   (c) A cloud occurring as shed vortex cavitation, sometimes merging into vortex group cavitation S, performing a separate collapse downstream the sheet cavity, frames 976–1132 in Fig. 5 and frames 2–7 in Fig. 1.
2. Compression rebound of a cavity, as in frame 12 of Fig. 4(b) and frame 1138 in Fig. 5.

Limiting cases of glassy secondary cavitation can occur, as the compression rebound in Fig. 8 and disintegration of thinning wavy cavities.

Secondary cavitation can be the creation of new cavitating volume from new nuclei, mixed with a transformation of an already existing cavity and re-opening of cavity residues downstream of a collapse, the latter shown in frame 7042 of Fig. 7. Usually a secondary cavity is of cloud type, frame 7072 of Fig. 7. Secondary cavitation can alone, or in interaction with a primary cavity, form a focusing cavity and

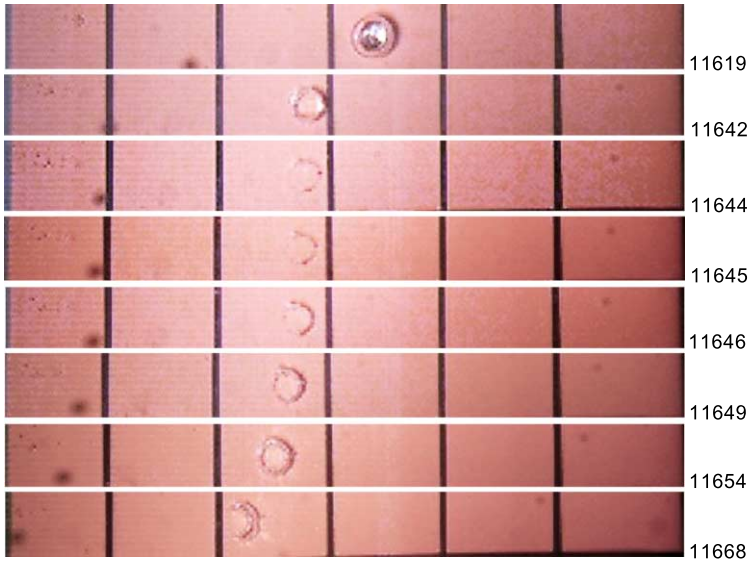

Fig. 8. An almost symmetric collapse and compression rebound to a glassy secondary cavity of a travelling bubble on an oscillating foil. The first collapse and rebound, lasting up to frame 11,654, are almost symmetric while an asymmetry is clearly visible in the collapse starting in frame 11,668. Flow from right to left. Chord length of foil is 120 mm, 12,000 frames/s. SSPA cavitation tunnel. From Bark et al. [3]. (Colors are visible in the online version of the article; http://dx.doi.org/10.3233/ISP-130097.)

generate erosion. Primary and secondary clouds can coexist in the same cavity, as in Fig. 2(a), where primary cloud streaks are generated far upstream, and later merge with secondary clouds generated by the re-entrant jet flow in the downstream region. Only sometimes can primary and secondary cloud cavitation be discriminated.

5. Asymmetry and vortex formation

Asymmetric collapses and the related vortex formation can have a significant influence on erosion. An early analysis of asymmetric collapses was made by Benjamin and Ellis [4] and the subject has later been discussed by other authors. An example is the experiment by Van der Meulen and Van Renesse [22] showing the influence of the flow velocity on a collapsing cavity close to a wall. As a basis for the present analysis of collapse asymmetry we consider first the travelling bubbles on an oscillating foil, Figs 8 and 9, and the attached sheet cavity in Fig. 10.

Figure 8 shows a collapse and compression rebound of a travelling bubble on an oscillating foil in a region with a small streamwise pressure gradient. The bubble is flattened from above and performs a first collapse and rebound as a glassy torus, with a minimum size just after frame 11,644. The almost conserved shape, glassiness

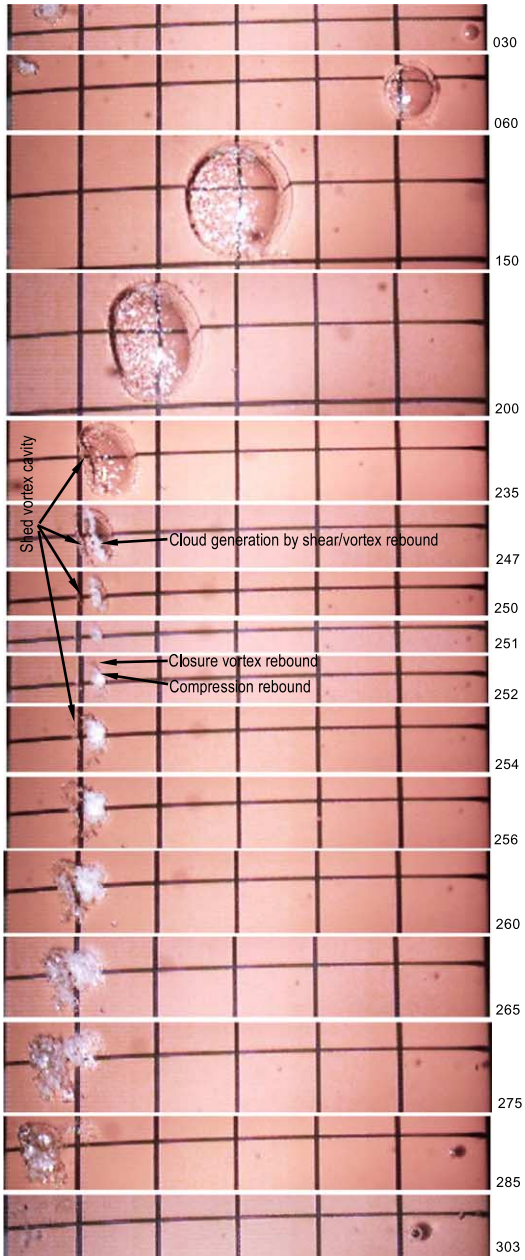

Fig. 9. Asymmetric collapse of travelling bubble and generation of a vortex rebound. Flow from right to left, oscillating foil, 12,000 frames/s. Same condition as in Fig. 8. SSPA cavitation tunnel. From Bark et al. [3]. (Colors are visible in the online version of the article; http://dx.doi.org/10.3233/ISP-130097.)

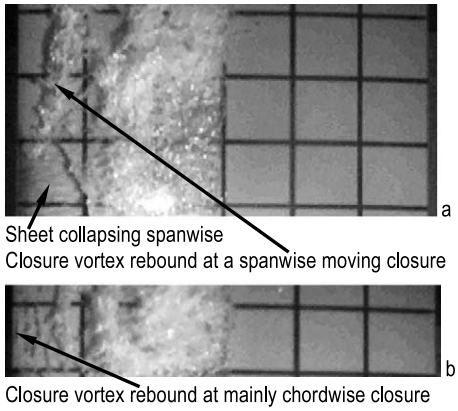

Fig. 10. Two different closure vortex rebounds. (a) The sheet cavity attached to the leading edge of an oscillating foil generates a "closure vortex rebound" due to the spanwise moving collapse. Flow from left to right. (b) The far left vortex cavity is a "closure vortex rebound" resulting from the final closure of the upstream moving sheet collapse. Downstream of this vortex does vortex group cavitation develop. See also the similar case in Fig. 12(g). Both these types of closure vortex rebounds, and some compression rebounds as well, occur close to the leading edge in the propeller case shown in Fig. 5. SSPA cavitation tunnel. From Bark et al. [3].

and the lack of shedding indicate that no noticeable vortex motion is created during the collapse and rebound. Nor is the collapse violent enough to trigger the cavity to rebound as a cloud. The rebound is completed in frame 11,654. After the next collapse and rebound, starting in frame 11,668, the bubble becomes increasingly asymmetric, due to a streamwise increasing pressure.

In Fig. 9 is shown a bubble collapsing in a region of streamwise increasing pressure. The downstream edge of the bubble has almost stopped moving in frame 235. A jet-like flow fills the bubble from its downstream end, resulting in shear and cloud cavitation, and shedding of a small vortex in frames 235–247. A glassy spanwise extending part of the bubble with the cloud in the center still exists in frame 250.

The collapse symmetry may increase in the end but it cannot be excluded that still some asymmetry influences the final collapse of the bubble, just after frame 251, resulting in a cavitating "*closure vortex*". Such a vortex also occurs due to spanwise collapse motion of a 3D cavity. The secondary cavitation created in this vortex is here referred to as a *closure vortex cavity* or, according to Analysis model 7, a "*closure vortex rebound* (*of the primary cavity*)". This is visible in frame 252 in Fig. 9, outside the intensely white core interpreted as mainly a compression rebound.

In frame 254 the shed vortex cavity has rebounded as a partly glassy cavity, indicating a slow collapse. Continued interaction between rebounding cavities and the recovering flow results in a "*continued vortex rebound*", shown in frames 254–285. Other examples of closure vortex rebounds due to spanwise collapse motions are shown in Fig. 10(a) for an attached sheet cavity and in Fig. 11 for a travelling sheet.

Analysis model 7 summarizes some basics.

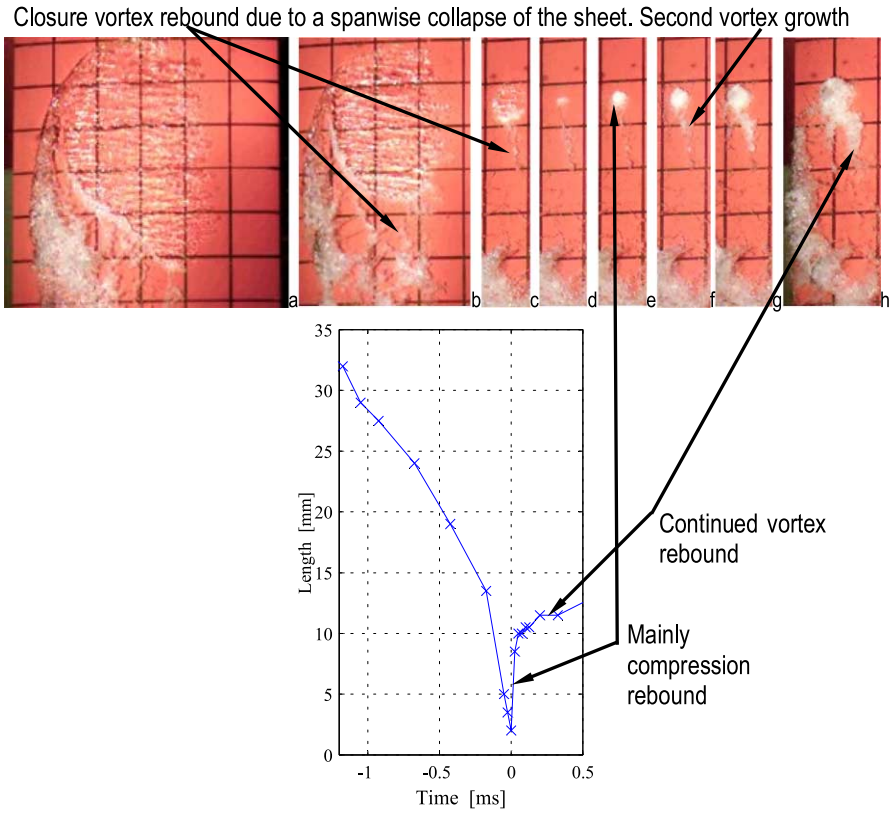

Fig. 11. Approximately symmetric final collapse of a sheet cavity on an oscillating foil. Flow from right to left, 5 m/s. The early part of the rebound is mainly a compression rebound. A slow *continued* vortex rebound occurs at times >0.1–0.2 ms. Plot of streamwise cavity length is based on a video of 40,000 frames/s. SSPA cavitation tunnel. From Bark et al. [3]. (Colors are visible in the online version of the article; http://dx.doi.org/10.3233/ISP-130097.)

Analysis model 7 (Collapse asymmetry and vortex formation). Almost streamwise symmetric collapses of travelling cavities can develop in flows with small streamwise pressure gradients, as for the travelling sheet cavity in Fig. 4.

For attached or traveling sheet cavities, as shown in Figs 4, 5, 7 and 11, the streamwise asymmetry of the collapse motion and the related formation of vortices are controlled by:

1. *The motion of the cavity detachment line*.
2. *The motion of the cavity closure region, including re-entrant jet flow*.
3. *The geometrical symmetry of the cavity*, particularly of the detachment and closure regions, as they approach each other in the collapse motion.

Important for the motion symmetry is *synchronization* of the collapse motion of different parts of a cavity. Lack of synchronization can split the collapse motion into parts, as filling of the cavity by jet flow before the onset of a pressure forced collapse. See also point 2 of Analysis model 2.

Asymmetry is a main reason behind development of secondary cavitation and the flow fields and geometry following from points 1–3, combined with the external flow, result in formation of spanwise vortices and, if the pressure admits, the following secondary vortex cavitation/rebounds:

4. *Vortex rebound of a cavity, by early shedding of independent vortex cavities or vortex group cavitation*, Fig. 7 frame 7042, Figs 5 and 10(b).
5. *Closure vortex rebound of a cavity, due to spanwise and chordwise collapse motions*. The process emanates from the collapse asymmetry and related shear and vortex formation at the closure of the primary cavity, explained by Fig. 12 and exemplified in Fig. 9 frames 251–252, Figs 10(a)–(b), 11(b)–(c) and (e)–(f).
6. *Continued vortex rebound of a cavity*, due to the shear and pressure conditions in the recovering flow, after the collapse of the primary cavity. Examples are shown in Fig. 1 frames 3–6, Fig. 7 frames 7072–7112 and Fig. 11(h).

When shedding occurs from a convex sheet cavity the vortices may transform into horse-shoe vortices that can enhance the focusing by the vortex cavity and the risk of erosion (point 4 in Analysis model 2).

In experiments the closure vortex rebound cannot always be isolated from the compression rebound. Therefore, an implicit LES for incompressible flow without permanent gas in the cavities is used for numerical prediction of some characteristics of a closure vortex rebound. Although the simulation does not represent the full physics the results shown in Fig. 12(a)–(f) for the upstream moving collapse of the attached sheet cavity on a NACA 0015 foil are in good agreement with observations. This condition generates a collapse that is similar to those shown in Figs 5 and 10. Figure 12(a)–(f) shows the finishing of the collapse of the primary sheet cavity and the shedding of vortex group cavitation starting before frame (g) in Fig. 13. The frames (a) and (b) show the penetration into the sheet cavity of a reversed flow induced by already shed vortices still existing downstream, frame (g) of Fig. 13.

By shear and momentum interaction between the penetrating jet and the flow outside the sheet cavity a vortex is formed at the upper corner of the "open" closure region of the sheet [8]. An amount of vapor from the sheet cavity is captured by the vortex, but condensates partly and temporarily, as is observed also in experiments, e.g. in the case of Fig. 7. In frame (c) three such vortices are created, and a new vortex appears upstream. In frame (d) the last cavitating vortex is created at the upstream end during the final filling of the sheet. The last two vortices join into a cavitating vortex elevating itself to the outside of a still upstream moving liquid layer, frame (e) and the enlarged view in frame (g). This joined vortex cavity is interpreted to be the

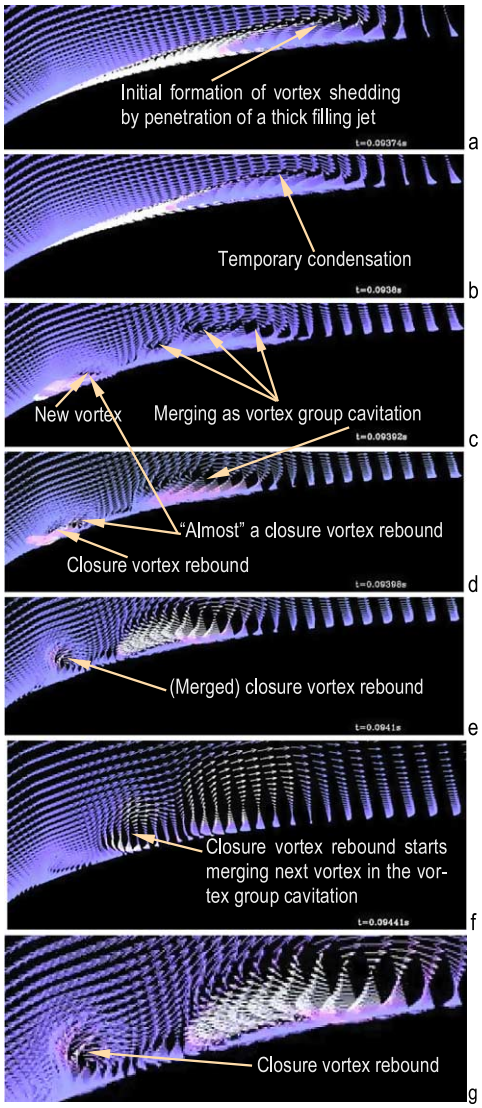

Fig. 12. Implicit 2D ILES, Lu [18]. White velocity vectors represents pure vapor. Simulation of the late part of the upstream moving collapse of an attached sheet cavity on a 2D NACA 0015 foil in stationary flow from left, at 8° angle of attack and cavitation number $= 1.2$. (a)–(c) Formation of vortex shedding and vortex rebounds in the downstream region. (d)–(f) Formation of a closure vortex rebound close to the sheet cavity detachment point. (g) Enlarged frame (e) showing the closure vortex rebound. From Bark et al. [3]. (Colors are visible in the online version of the article; http://dx.doi.org/10.3233/ISP-130097.)

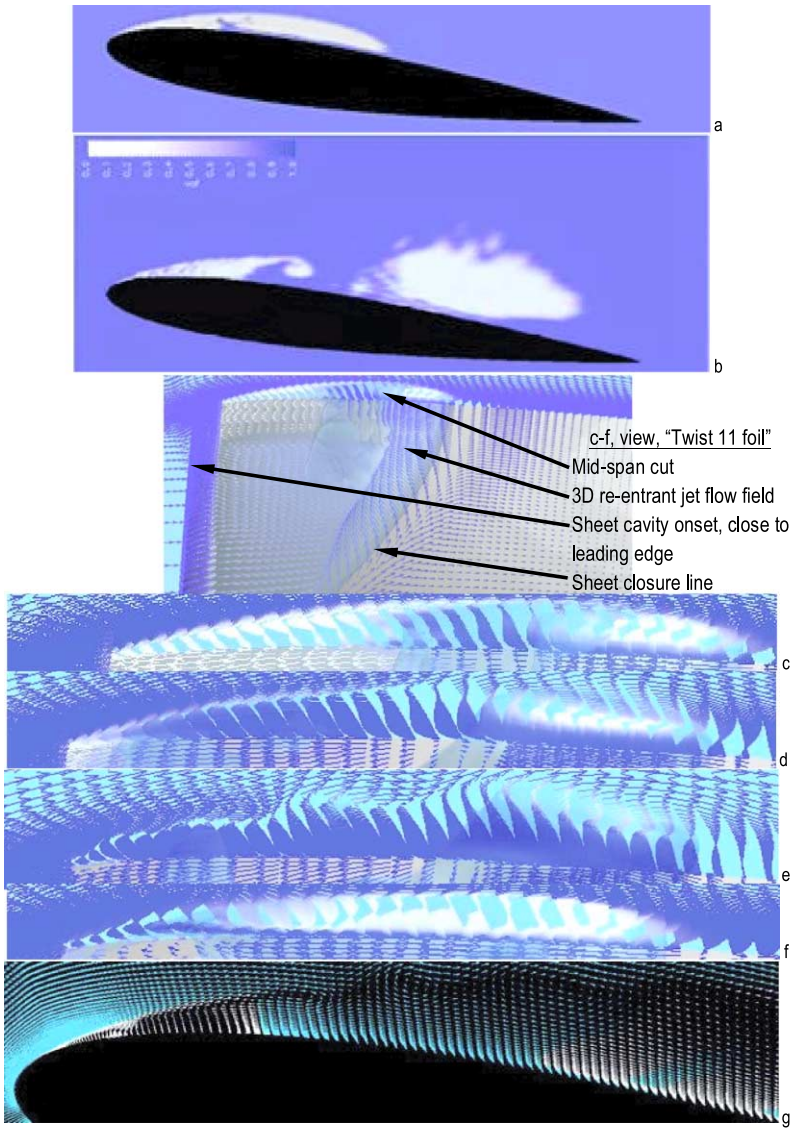

Fig. 13. Filling flows of jet-type. Simulations with ILES. White is vapor and blue is water. (a) 2D foil and simulation, re-entrant jet accumulating upstream. (b) As (a), but with a thick jet, induced partly by the shed vortex cloud. (c)–(f) Twisted 3D foil [8]. (c)–(e) Velocity profiles showing accumulation of liquid inside the sheet cavity due to the filling by a converging re-entrant jet flow. (f) Thin re-entrant jet reaching the leading edge. (g) Filling by a thick jet, due to shed vortices or separation on 2D, NACA15 foil, 2D simulation. (a) and (b) simulation by Wikström [23], (c)–(f) by Huuva [14] and (g) by Lu [18]. Frames from Bark et al. [3]. (Colors are visible in the online version of the article; http://dx.doi.org/10.3233/ISP-130097.)

cavity that can be observed also in experiments, and be identified as a closure vortex rebound. The vortex travels downstream and joins the next downstream vortex, frame (f). The local rising visible in frame (e) can be imagined in frames 994–1010 in Fig. 5. Finally all vortices typically join, as in Figs 1 and 5, frame 1090.

By the lifting of the collapse point from the body and dispersing the collapse in time and over a larger area, the vortex rebound has a potential to reduce erosion. An important issue for particularly experimental assessments is to what extent the compression rebound can be safely discriminated from a closure vortex rebound, and be used as an indicator of potentially erosive collapses. The present experiments and simulation indicate that the durations of the different early rebounds may be of the same order, and that discrimination then may be difficult.

In the bubble collapse in Fig. 9, frame 252, where closure vortex and compression rebounds are overlapping, it seems possible to discriminate the compression rebound by its high density of small bubbles, and possibly also faster growth. This tendency that the central part of the rebound is more white and explosive, and thus believed to be mainly a compression rebound, occurs in the condition in Fig. 11 as well. A superimposed closure vortex rebound can still not, however, be excluded.

Experiences from EROCAV indicate that a fast rebound is an erosion indicator. The present study does, however, indicate that this hypothesis would be checked, particularly for clearly asymmetric collapses, as in Fig. 5 for which the possible misinterpretation may result in over prediction of the erosion risk. As will be commented below the second growth/rebound of the vortex cavity in frame (f) of Fig. 11 may be initiated or enhanced by the rarefaction phase of the sheet cavity rebound pulse.

6. Generalized collapse and rebound

To highlight losses of energy that may contribute to erosion and to extend the view of a cavity rebound we finally introduce the concepts of generalized collapse and rebound. As a reference we define the simple collapse of a focusing cavity:

Analysis model 8 (The simple collapse). A collapse of a focusing cavity, e.g. a sheet cavity, is called a simple collapse if it holds that:

1. The collapse motion is forced by the surrounding pressure only, controlled by the incoming flow and global pressure.
2. The collapse symmetry results in a mainly elastically controlled collapse stopping, thereby generating a compression rebound of the cavity.
3. The loss of focusing volume or collapse energy focusing due to the following processes is negligible:
   (a) Vortex formation due to a major collapse asymmetry.
   (b) Filling of the cavity by re-entrant jet flow or similar flows, which are not synchronized with, and are not parts of, the essential collapse flow that is finally filling the cavity.

(c) Disintegration of the focusing cavity.
(d) A partially and temporarily reduced or reversed collapse acceleration or velocity resulting in an "interrupted collapse", due to a temporal change of the incoming flow.

This definition of the simple collapse indicates ways by which the erosion efficiency of a cavity can be reduced and it is in this sense a basis for collapse analysis. The basic example and limiting case of a simple collapse is the spherically symmetric collapse of a cavity containing some gas, the compression of which may contribute to the rebound motion. A symmetric collapse of a sheet cavity can approach this behavior and the high focusing efficiency of the spherical collapse. Examples of cavities approaching a simple collapse are the sheet cavity A in Fig. 4(a) and the one shown in frames 7042–7063 of Fig. 7.

As regards the losses, which are negligible for the simple collapse, the points 3 (b) and (c) are straightforward. The vortex formation addressed in point 3 (a) brings a loss of energy focusing, exemplified by the difference between the collapses of a spherical cavity in an unbounded environment and the collapse of an initially spherical cavity close to a wall. Because of the asymmetry developing during the latter type of collapse, the energy will be dispersed, by a jet impact into the liquid and formation of a vortex cavity.

The asymmetric and upstream moving collapse of the sheet cavity in Fig. 5 generates closure vortex rebounds and possibly some tiny compression rebounds close to the leading edge. The collapse front, mainly a thick jet filling, moves upstream with a slowly increasing velocity, close to the free stream velocity (Fig. 5 in [11]). This flow results in a spanwise scattered and slightly weak energy focusing. As shown by Fig. 1 a change of the condition, adding also a spanwise focusing, can make the sheet focusing erosive in the upstream region.

Jet fillings of different types are shown in Figs 12 and 13. In the 2D cases in Fig. 12 and frames (b) and (g) of Fig. 13 the jet filling is the only flow creating the collapse, because the angle of attack and global pressure are constants. The thick jets sometimes spanning the entire cavity thickness, as in frames (b) and (g) of Fig. 13, often have their origin in a separated flow or in the existence of shed vortices downstream of the sheet. The vector plots indicate that the filling flow typically has an approximately constant velocity during a large part of the filling and does then not accelerate the collapse, as happens for a free pressure-forced collapse. This non-accelerating filling corresponds to a loss of collapse energy.

Point 3(d) refers to the frequently occurring situation that the collapse during some time is forced, by a variable incoming flow, to proceed at reduced, constant or even reversed velocity rate, compared to a monotonous acceleration for the "free" collapse, forced by a constant pressure. If for example the collapse motion is stopped and then restarts, due to the wake field, the energy related to the first part of the collapse is missing in the restarted collapse. Usually only a small part of the initially available potential energy may end up in the highly synchronized collapse motion

needed for erosion. In a kinematically based assessment of the energy focusing, it is important to capture how the initially available potential energy is redistributed during the collapse into kinetic energy.

Significant loss of focusing cavity volume can occur by disintegration of the focusing cavity into parts. Shed parts can form new erosive focusing cavities, as the early shedding of the cavity B in frame 5 of Fig. 4(a), but they can alternatively collapse without significant energy focusing and erosion risk. A very late disintegration of an early formed, large secondary cloud is shown in frame 7 in Fig. 1. The frame 1 in Fig. 1 shows the disintegration of the primary sheet cavity into two focusing collapses of glassy parts. Disintegration by local disappearance of a sheet cavity, due to locally increased pressure, is a typical mechanism by which the focusing root cavity in frame 7046 in Fig. 7 is created from a large sheet cavity.

The thick jets mentioned below Analysis model 8, often spanning the entire cavity thickness and shown in frames (b) and (g) of Fig. 13 are of particular interest. As stated above the source of this thick jet is a separated flow or existence of shed vortices downstream of the sheet. In frame (g) of Fig. 13, continued in Fig. 12, it is shown how this type of jet can in the limit totally fill a sheet cavity, without an increase of the global pressure. In this case there is no simple collapse forced by the environmental pressure.

As remarked, a full height jet front can still accelerate and generate energy focusing – resulting in at least a closure vortex rebound, and probably also an amount of compression rebound and erosion.

When a jet enters the downstream part of a sheet cavity and initiates the formation of a vortex a temporary stagnation point develops in the closure region of the sheet cavity, Fig. 12, frames (a) and (b).

For interpretation of the experimental observations of collapses and rebounds of shed cavities we recall some fundamentals of the spherically symmetric collapse, based on the simulations by Hickling and Plesset [13]. We assume that some general trends, as the late collapse pulse generation, for this basic case are approximately similar also for sheet cavities. For example is a significant part of the non-dimensional collapse history of the freely advected and collapsing sheet cavity in Fig. 4 fairly similar to the spherically symmetric case [11].

According to classic theory a collapsing empty spherical cavity generates in the limit of vanishing an infinitely high collapse pulse at the distance $1.59R$ from the cavity center, with R being the cavity radius. This collapse is not retarded by compression of a gas inside the cavity, or by any other force acting from the inside on the cavity interface. It is also noted that the maximum of the collapse induced pressure occurs inside the liquid and accordingly this pulse is a pure inertial effect, related to the converging flow. This pulse, here called the "inertial collapse pulse", starts to develop early during the collapse, at distances $>1.59R$, and with high amplitudes only towards the end of the collapse.

For the analysis of some experimental data we assume that the inertial pulse may in principle force a nearby cloud to collapse, before gas compression stops the collapse

of the focusing cavity and thereby initiates a stopping pulse that otherwise will force the cloud collapse.

Existence of rebounds in also rather slow or moderately fast collapses, as the example in Fig. 8, supports, however, the idea that at least also gas compression can contribute to typical collapse stopping motions and related collapse stopping pulses.

In the first frame of Fig. 7 the collapse of the focusing cavity, i.e. the glassy primary sheet cavity with its attached secondary cloud, is approaching its end as the blade leaves the wake peak. We assume that the pressure forcing the collapse and rebound of the cavities that are shed from the sheet cavity in this generic case is typically a superposition of some of the following parts:

(a) The *globally controlled pressure* on the blade, varying with blade position.
(b) The *stagnation pressure*, downstream of a sheet cavity, related to re-entrant jet flow and shedding.
(c) The *inertial collapse pulse*.
(d) The final *collapse stopping pulse* from the sheet cavity collapse, assumed to be controlled by gas and liquid compression, or in some cases by a water hammer impact on the body surface.
(e) The *rarefaction phase* of the stopping pulse (d), developing during the retardation of the rebound motion, often enhanced by the pressure in a recovering flow.

The main erosion at the condition in Fig. 7 is created by the collapse after frame 7063 of the sheet cavity, including the attached cloud. The collapse triggers the development of the large secondary cloud in frame 7112, a cloud forming a separate focusing cavity that performs an erosive collapse after frame 7199.

The flow filling the sheet cavity from right in frame 7042 is assumed to be a combination of an early re-entrant jet and a collapse motion forced by the global pressure. A number of small vortex cloud cavities, A, B, C and D, are shed from the attached cloud. Cavity A is actually a group of cavities while the others are mainly single vortex cavities. The following observations and interpretations are made:

1. A short time after shedding, the cavities are suppressed, slightly fluctuating in size, or making a complete collapse and rebound. The time resolution, (1/75,000 s) is, however, too low to reveal the details. There are some later fluctuations as well, which are weak and not fully resolved. The suppression and motion of the shed cavities may be forced by a combination of the inertial collapse pulse close to the attached cloud, the unsteady stagnation pressure and the global pressure. Frame 7063 is the last frame showing the glassy part of the sheet cavity (the arrowheads point at the upstream and downstream edges of the last traces of the glassy part).
2. The early phase of the compression rebound of the sheet cavity is visible in frame 7064, the intensely white cloud. In this frame the latest shed cavity, D, has almost collapsed and cavity C and the surrounding cloud are suppressed.

The suppression of the shed cavities spreads downstream from the collapse point, assumed to be forced by the collapse and rebound pulse from the sheet cavity.

3. In frame 7065 the collapse pulse suppression has reached the cavity groups A and C that have almost disappeared. Cavity B has totally collapsed. The diluted cloud that was distributed over the collapse wake is also gone. The outward spreading rebound, assumed to still be forced by the rarefaction phase of the rebound pulse from the sheet collapse, has expanded cavity D and created some diluted cloud that has reached cavity C.
4. In frame 7066 the rebound has reached cavity B and the left part of cavity A. The right part of cavity A is further suppressed and the thin cloud downstream of cavity A has condensed, forced by the outwards spreading sheet collapse pulse.
5. In frame 7067 the rebound has reached the region downstream of cavity A. The rebound in the sheet collapse point is now very strong, almost explosive. This continues to at least frame 7072 where some of the originally shed cavities can still be identified. The cloud is spreading upstream and outwards from the blade surface, combined with a strong interaction with the incoming flow in the upstream cloud front.
6. A very striking feature up to frame 7072 is the slow advection of the shed cavities. During a short time after shedding, the shed cavities are typically moving upstream. Cavity B is observable from frame 7056–7067 at virtually the same position on the blade. During this time a particle advected with the flow has moved approximately a double line-width of the propeller markings. After approximately frame 7072 the advection of the cloud adapts to the surrounding flow, and a rotational motion of the cloud groups can be imagined in the video. This behavior is assumed to result in further cloud generation in the recovering flow and global pressure after the sheet collapse.
7. The cloud finally undergoes an erosive collapse in frame 7199, dispersed in this blade passage into four collapse points.
8. Acoustic interaction forced by the collapse pulse is not limited to cavities in the collapse wake but because of the short duration of this pulse a significant influence will only appear on small cavities. Mainly small nearby clouds can be expected to collapse by this interaction. The influence of the rarefaction phase is more extended in time, as indicated by simulation of two acoustically interacting bubbles [12].

Observed with less time resolution the development between frames 7063 and 7112 would simply be called a rebound. The present resolution reveals the existence of a number of sub events and the process would rather be described as a "generalized rebound". A noticeable part is the effect of the recovering flow and pressure after the collapse of the sheet cavity. This effect on the growth of the cloud cavitation is significant after approximately frame 7072 in Fig. 7. Similar effects occur in all

presently studied propeller conditions and can also result in a re-growth of the sheet during a short time as the blade leaves the wake peak. Such a "false rebound" of the sheet cavity is shown in Fig. 5 frames 1090–1120.

Comparing the development in Fig. 7 with the slower and more asymmetric collapse of the sheet cavity in Fig. 5 we notice that during the early shedding there is in Fig. 5 a suppression of shed cavities, and occasionally also regular collapses and rebounds. The shed cavities reach after a short time a final moderate size, sometimes too small to merge into vortex group cavitation, frames 984–994. They are moving downstream and collapse as individual cavities, sometimes in an erosive way, but very scattered over the blade. Close to the leading edge, where the collapse speeds up, the development is approaching that in frame 7064 of Fig. 7.

An example of merging into vortex group cavitation occurs in frames 996–1050 in Fig. 5, to be compared with frames 7064–7112 in Fig. 7. This basic development appears in all sheet cavitation conditions presented in this paper, and can be traced in the case with the travelling bubble in Fig. 9 as well. The balances among different parts of the process are, however, different. In the condition in Fig. 5 the collapse pulse from the sheet cavity is for example much weaker than in the case of Fig. 7.

Based on the cases discussed above we define first the generalized collapse, addressing main events to look for, above the collapse symmetry.

Analysis model 9 (The generalized collapse). The focusing cavity under consideration can be a part of a glassy sheet cavity with an attached cloud, or a pure cloud cavity. As regards the energy focusing in a single collapse, the generalized collapse of a focusing cavity is composed of the processes:

1. *The simple collapse*, according to Analysis model 8, with the added complexity emanating from non-negligible effects of the mechanisms (a)–(d) in next point.
2. *Dissipative or dispersive collapse mechanisms*, reducing the collapse energy or focusing by reduction of the cavity volume or changing the kinematics:

   (a) *Vortex formation*, due to a collapse asymmetry that e.g. in the final collapse phase can reduce the energy focusing by creation of a closure vortex, as in the upstream moving collapse of an attached sheet cavity in Fig. 5, explained in Fig. 12(g).
   (b) *Filling of the cavity by re-entrant jet flow* or similar upstream moving flows, which are not synchronized with, and are not parts of the essential collapse flow that is finally filling the cavity. Examples: Fig. 2, the thick jet creating the attached cloud in Fig. 5, the different jets shown in Figs 12 and 13.
   (c) *Disintegration* of the focusing cavity. Examples: Frames 1 and 7 in Fig. 1, the upper 4 frames in Fig. 3, cavity B in Fig. 4(a), the sheet cavity in frames 7042–7063 and secondary cloud in frame 7199 of Fig. 7.
   (d) *Collapse interruption* (see comments on point 3(d) in Analysis model 8).

In the generalized collapse effects (a)–(d) may dominate over the simple collapse. Typically, erosive collapses result in rebounds into new erosive secondary cavities.

Due to the collapse asymmetry and jet formation often developing in flows, a rebound of a cavity in a flow can differ significantly from a rebound in a liquid at rest [22]. In Analysis model 6 it was suggested that secondary cavitation due to collapse motion can alternatively be interpreted as a kind of rebound, a part of a generalized rebound, and in Analysis model 7 the term "vortex rebound" of the primary cavity was introduced.

From Figs 9 and 11 we concluded that the compression and closure vortex rebounds can be difficult to discriminate, because of partial coincidence in space and time. The early structure and symmetry of the rebound flow may sometimes be an experimentally useful indications of the type of rebound. For example can a spherically symmetric spreading of a cloud of very small bubbles indicate a compression rebound, as in frame 7064 in Fig. 7, the central part of the rebounded cavity in frame 252 of Fig. 10 and frame (e) in Fig. 11. Analysis of the generalized rebound, i.e. the combined effects of vortex and compression rebounds addresses three main issues:

(a) The problem of using a compression rebound as indicator of erosive collapses, because the difficulty to discriminate it from fast vortex rebounds.
(b) The closure vortex rebound as indicator of reduced erosion risk.
(c) The compression and vortex rebounds as main sources of erosive cloud cavitation.

These points are reasons to capture as much as possible of the generalized rebound, in experiments and simulations. Based on the discussion in connection to the lists (a)–(e) and 1–8 before Analysis model 9 we formulate the Analysis model 10.

Analysis model 10 (The generalized rebound). The generalized rebound is defined as the superimposed compression and vortex rebounds of a sheet cavity and its shed cloud cavities, including a possible merging of the rebounded cavities. An example is the rebound of the sheet in frame 7042 in Fig. 7, starting in a sense already in frame 7042 but more clearly in 7063–7064 and finished in 7112.

This process is decomposed into two coupled main parts, the generalized rebound of the sheet cavity and the additional sub processes influencing the secondary clouds shed from the sheet:

The generalized rebound of a sheet cavity, including attached secondary clouds. The sheet cavity can be of any configuration in which re-entrant jets or similar flow may develop. The process is decomposed in the following way:

1. *Vortex rebound by jet filling of the sheet cavity* and related shear, generating secondary cavitation, shed as *single vortex cavities* possibly merging into *vortex group cavitation* and finally a single cloud, Fig. 1 frames 2–5, Fig. 7 frames 7042–7063, Fig. 5 frames 976–992 and Fig. 9 frame 247. Vortex rebound by jet filling is usually weak or non-existing in cloud sheets.

2. *Closure vortex rebound of the sheet cavity*, at the closure of the sheet in an upstream collapse point, Figs 10(b) and 12(g), or in a downstream collapse point, Fig. 9 frames 251–252, or in a spanwise moving collapse, Fig. 5 frames 994–1004, Fig. 9 frame 252, Figs 10(a) and 11.
3. *Compression rebound of the sheet cavity*, Fig. 3 frames 1133–1136, Fig. 4(b) frames 11–12, Fig. 7 frame 7064, Fig. 9 frame 252, appearing superimposed on the closure vortex rebound and Fig. 11 frame (e).
4. *Continued vortex rebound of the sheet cavity*, by the shear and pressure conditions in the recovering flow after points 1–3, Fig. 1 frames 4–5, Fig. 7 frames 7066–7112, Fig. 9 frames 254–265 and Fig. 11 frames (g)–(h).

Additional sub processes influencing shed secondary clouds, as the clouds A–D in Fig. 7. This development starts by point 5, when the collapse of the sheet cavity and the shedding according to point 1 are still going on:

5. *Compression rebounds of shed secondary clouds*, following on possible collapses after shedding, Fig. 1 frames 2–4 and Fig. 7 frames 7042–7067.
6. *Continued vortex rebound of shed secondary clouds*, by shear and pressure conditions in the recovering flow. This development starts after points 1–3 for the sheet cavity and is typically joined with point 4 for the sheet cavity, Fig. 1 frames 4–5, Fig. 5 frames 994–1090 and Fig. 7 frames 7065–7112.

Finally there is the compression and vortex rebound, after a possibly common collapse of the shed clouds and the rebounded sheet cavity, following after points 1–6, Fig. 1 frame 8, Fig. 5 frames 1132–1158 and Fig. 7 frame 7202 (only shed parts involved). After this sequence there may follow further collapses and rebounds of decaying intensities.

7. Summary and conclusions

It is certainly possible to describe the cavitation processes in Figs 1 and 7, in classic terms of bubble, sheet, vortex and cloud cavitation etc. The argument for introducing the present concepts is the possibility to make a more revealing analysis, improve understanding and address processes discriminating bad from good developments.

The concepts are condensed into ten conceptual Analysis Models, aimed to be applied to experimental or numerical data for highlighting development of large to medium–small scale events. At these scales the flow is still related to design parameters. The identified main processes are then:

1. Cascading of collapse energy from a glassy sheet cavity to cloud cavities.
2. Characteristic processes controlling erosion by cloud cavitation.
3. Focusing and cascading of collapse energy – focusing cavities and collapses.
4. Formation of focusing cavities.

5. Primary cavities.
6. Secondary cavities.
7. Collapse asymmetry and vortex formation.
8. The simple collapse.
9. The generalized collapse.
10. The generalized rebound.

The essential process is No. 3, about collapse energy focusing, while the other processes bring supplementary understanding about why and how erosive cavity configurations are created and how cascading and focusing of collapse energy proceed. The introduced concepts are aimed to isolate and highlight the crucial events in the hydrodynamics of cavitation erosion and constitute a nomenclature for analysis and communication. The present analysis principles extend the analysis procedures and ideas presented by Bark et al. [1] and Grekula and Bark [11].

The list of Analysis Models defines a set of main processes. This list does not, however, reflect a typical time sequence of the cavitation development. Some processes are overlapping and can occur more than once during a cavitation cycle. There also exist some overlap and coupling between the introduced definitions and processes. The reason is the complexity of the total cavitation process, and the fact that similar developments can sometimes be reached in different ways and from different initial cavity configurations. The complexity developing also from an initially simple event is exemplified by the compression rebound that triggers a series of sub processes creating shear and momentum interactions as well as acoustic interaction, frames 7064–7202 in Fig. 7. The sub processes create additional secondary cloud cavitation that is added to the cloud generated by the initial rebound. The existence of parallel and interacting chains of coupled sub events and processes is indicated in Analysis models 9 and 10.

The selection of scales to be analyzed reflects the aim to understand the development from sheet cavitation towards erosive collapses. This means tracing of the kinematics, up to and including ideally a state corresponding to frame 9 in Fig. 4(b). Together with observation of the rebound this allows an estimate of the unresolved continuation, the small-scale and fast "micro focusing", resulting in the impact on the body surface that creates the material damage.

The final collapse pulse, generated between frames 9 and 11 in Fig. 4(b), is assumed to be strongly enhanced by the focusing motion before frame 9, which can be traced back to the early global development shown in the first frames in Fig. 4(a). This enhancement of the cloud collapse by a sheet cavity collapse is a basic hypothesis in the present approach. Considering the sheet and the attached or nearby cloud as a single degenerated cloud containing in addition to the small bubbles also one very large bubble, this hypothesis is actually a special case of the collective collapse of interacting bubbles.

In a sense the presented approach describes the formation of the initial conditions for the very last hydrodynamic energy focusing and the generation of the final collapse phase and the damaging impact on the solid body.

The height and steepness of the final collapse pulse are also influenced by the amount of permanent gas and bubble distribution in the cloud starting its collapse in frame 9 of Fig. 4(b). Such parameters are, however, influenced by local liquid conditions and are less uniquely related to large-scale flows and design.

The influence of the local liquid properties on the collapse pulse means difficulties with interpretation of collapse pulses that are numerically simulated or measured at a model experiment. Simulations of bubble collapses demonstrate a high sensitivity for assumptions about the bubble content. Still simulation and measurements of such pulses can be useful for relative comparisons of alternative designs and for correlation with experimental erosion data.

Numerical simulation of collapse pulses on the body surface corresponds in a sense to paint tests in model experiments. For erosion risk prediction only, collapse pulses or paint test may be relevant and sufficient, but for understanding design selections, an analysis of the cavity dynamics is useful.

If the very final collapse and the related pulse cannot be captured with sufficient resolution an approximate erosion risk assessment could be made, based on the early collapse focusing. However, the early collapse focusing is usually less reliable. Already by frame 3 of Fig. 4(a) it can be stated that there is a clear risk for severe erosion, which actually happens in the shown case. It can, however, also be demonstrated that proper design of propeller and wake can transform a cavity of that early appearance to a non-focusing cavity, disappearing without any generation of erosion.

Acknowledgements

The presented work is finished under the European Union project Hydro Testing Alliance (HTA), JRP6, with input from the earlier European projects VIRTUE and EROCAV. Parts of the simulations are made with support from the Rolls-Royce University Technology Center at Chalmers, The Swedish Armed Forces (FM) and The Swedish Defense Research Agency (FOI).

References

[1] G. Bark, N. Berchiche and M. Grekula, Application of principles for observation and analysis of eroding cavitation, EROCAV observation handbook, Ed. 3.1, Department of Shipping and Marine Technology, Chalmers University of Technology, Sweden, 2004, available at: www.chalmers.se/smt.

[2] G. Bark, M. Grekula, E.R. Bensow and N. Berchiche, On some physics to consider in numerical simulation of erosive cavitation, in: *Proceedings 7th International Symposium on Cavitation*, CAV2009, Ann Arbor, MI, USA, August 17–22, 2009, pp. 677–692.

[3] G. Bark, M. Grekula and N.-X. Lu, Analysis of erosive cavitation by high speed video records, in: *Proceedings 2nd International Conf. on Advanced Model Measurement Technology for the EU Maritime Industry*, Newcastle University, Newcastle, UK, 4–5th April, 2011, pp. 33–49.

[4] T.B. Benjamin and A.T. Ellis, The collapse of cavitation bubbles and the pressure thereby produced against solid boundaries, *Royal Soc. London, Philosophical Transactions A* **260** (1966), 221–240.

[5] R.E. Bensow and G. Bark, Implicit LES predictions of the cavitating flow on a propeller, *J. Fluids Engineering* **132** (2010), 041302-1.
[6] R.E. Bensow, T. Huuva, G. Bark and M. Liefvendahl, Large eddy simulation of cavitating propeller flows, in: *27th Symposium on Naval Hydrodynamics*, Seoul, Korea, 2008, pp. 229–249.
[7] A. Boorsma and P. Fitzsimmons, Quantification of cavitation impacts with acoustic emissions techniques, in: *Proceedings 7th International Symposium on Cavitation, CAV2009*, Ann Arbor, MI, USA, August 17–22, 2009, pp. 84–89.
[8] E.-J. Foeth, The structure of three-dimensional sheet cavitation, PhD thesis, Delft University of Technology, Delft, The Netherlands, 2008.
[9] M. Fukaya, Y. Tamura and Y. Matsumoto, Prediction of cavitation intensity and erosion area in centrifugal pump by using cavitating flow simulation with bubble flow model, *J. Fluid Science and Technology* **5**(2) (2010), 305–316.
[10] M. Grekula, Cavitation mechanisms related to erosion; studies on Kaplan turbines, foils and propellers, PhD thesis, Department of Shipping and Marine Technology, Chalmers University of Technology, Göteborg, Sweden, 2010.
[11] M. Grekula and G. Bark, Analysis of high-speed video data for assessment of the risk of cavitation erosion, in: *Proceedings 1st International Conf. on Advanced Model Measurement Technology for EU Maritime Industry* (AMT09), Nantes, France, 1–2 September 2009, pp. 83–100 (also included in [10]).
[12] J. Hallander and G. Bark, Influence of acoustic interaction in noise generating cavitation, in: *24th Symposium on Naval Hydrodynamics*, Fukuoka, Japan, July 8–13, 2002, pp. 879–895.
[13] R. Hickling and M.S. Plesset, Collapse and rebound of a spherical bubble in water, *Physics of Fluids* **7**(1) (1964), 7–14.
[14] T. Huuva, Large eddy simulation of cavitating and non-cavitating flow, PhD thesis, Chalmers University of Technology, Sweden, 2008.
[15] ITTC, The Cavitation Committee report, in: *Proceedings of the 20th International Towing Tank Conference*, Vol. 1, The University of California, San Francisco, CA, USA, 1993, pp. 191–255.
[16] ITTC, The Cavitation Committee report, in: *Proceedings of the 21st International Towing Tank Conference*, Vol. 1, The Norwegian University of Science and Technology Trondheim, Norway, 1996, pp. 63–126.
[17] Z.R. Li, Assessment of cavitation erosion with a multiphase Reynolds-averaged Navier–Stokes method, PhD thesis, Delft University of Technology, Delft, The Netherlands, 2012.
[18] N.-X. Lu, Large eddy simulation of cavitating flow on hydrofoils, Licentiate thesis, Department of Shipping and Marine Technology, Chalmers University of Technology, Gothenburg, Sweden, 2010.
[19] N. Ochiai, Y. Iga, M. Nohmi and T. Ikohagi, Numerical prediction of cavitation erosion intensity in cavitating flows around a Clark Y 11.7% hydrofoil, *J. Fluid Science and Technology* **5**(3) (2010), 416–431.
[20] S.J. Schmidt, M. Thalhamer and G.H. Schnerr, Inertia controlled instability and small scale structures of sheet and cloud cavitation, in: *Proceedings 7th International Symposium on Cavitation, CAV2009*, Ann Arbor, MI, USA, August 17–22, 2009, pp. 62–75.
[21] J. Schöön and G. Bark, Some observations of violent collapses of sheet cavities and subsequent cloud cavitation on a foil in unsteady flow, in: *Proceedings ASME Fluids Eng. Summer Meeting*, Washington, DC, USA, June 22–25, 1998, paper FEDSM98-5068.
[22] J.H.J. Van der Meulen and R.L. Van Renesse, The collapse of bubbles in a flow near a boundary, in: *17th Symposium on Naval Hydrodynamics*, The Hague, The Netherlands, August 28–September 2, 1988, pp. 397–392.
[23] N. Wikström, Approaching large eddy simulation of cavitating flows for marine applications, PhD thesis, Department of Shipping and Marine Technology, Chalmers University of Technology, Gothenburg, Sweden, 2006.